*32nd EPS Conference on Plasma Phys. Tarragona, 27 June - 1 July 2005 ECA Vol.**29C**, P-4.040 (2005)*

Analysis of ELM heat pulse propagation in the JET scrape-off layer with an integrated fluid-kinetic approach

J.-S. Lönnroth[1], G. Corrigan[2], W. Fundamenski[2], V. Parail[2], J. Spence[2], D. Tskhakaya[3*] and JET-EFDA contributors[**]

[1]*Association EURATOM-Tekes, Helsinki University of Technology, Finland*
[2]*EURATOM/UKAEA Fusion Association, Culham Science Centre, United Kingdom*
[3]*Association EURATOM-ÖAW, Innsbruck University, Austria*
[*]*Permanent address: Institute of Physics, Georgian Academy of Sciences, Tbilisi, Georgia*
[**]*See the Appendix of J.Pamela et al., Proc. 20th Int. IAEA Fusion Energy Conf., 2004.*

1. Introduction. Transport in the scrape-off layer (SOL) is poorly understood, especially during transients such as ELMs. Generally, ELMs give rise to large particle and heat loads at the divertor plates, because the parallel transport along the field lines usually dominates over perpendicular transport across the field lines. Since the parallel motion along the field lines is limited to the convective speed of the particles, separate distinct heat pulses first due to electron heat transport and later due to ion heat transport are first registered at the outer target and subsequently at the inner target, to where the distance along the field lines is greater in the usual case of ELMs occurring at the outer midplane. At JET, the propagation time of the ion heat pulse to the outer target has been measured to be of the order of 100 μs, with the ion heat pulse to the inner target being delayed by roughly a further 200 μs. In this paper, the propagation of a heat pulse induced by an ELM at the outer midplane is studied with an integrated fluid modelling approach, which is eventually complemented by kinetic simulations due to the insufficiency of the fluid approach alone.

2. Method. The main tool used in this study is the integrated transport code COCONUT, which is a self-consistent coupling of the 1.5D core transport code JETTO [2] and the 2D edge transport code EDGE2D / NIMBUS [3]. In a COCONUT run, JETTO calculates the heat fluxes and transport coefficients in the core and passes their values at the separatrix as boundary conditions for EDGE2D, whereas EDGE2D calculates the corresponding quantities in the SOL and passes their separatrix values as boundary conditions for JETTO [4]. The boundary between the 1D JETTO grid and 2D EDGE2D grid is here at the separatrix and both codes are called at each time step. The edge transport barrier (ETB) is represented by a suppression of all perpendicular transport coefficients to a uniform ion neo-classical level in a narrow region just inside the separatrix on the one-dimensional grid. Inter-ELM perpendicular transport in the SOL, where the grid is two-dimensional, is kept constant at the same level as in the ETB. Parallel transport in the SOL is calculated according to the 21-moment approximation [5]. The parallel transport coefficients can be scaled by adjusting the transmission factors α_i and α_e in the so-called flux limiter, defined as

$$\chi_{\parallel s} = \frac{\chi_{\parallel,0s}}{1+\left|\dfrac{n_s \chi_{\parallel,0s} \nabla T_s}{\alpha_s n_s c_s T_s}\right|}, \qquad (1)$$

which describes the transition from diffusive to convective transport. Here, the subscript *s* refers to either ions or electrons, $\chi_{\parallel 0}$ is the parallel thermal conductivity given by the 21-moment approximation, *n* is the density, *T* is the temperature and *c* is the sound speed. In the simulations in this paper, the transmission factors default to $\alpha_i = \alpha_e = 0.2$.

A high-density pure deuterium plasma has been chosen for the analysis. A heat pulse is induced at the outer midplane by increasing the perpendicular transport coefficients in the following way: In the ETB at the edge of the 1D grid, perpendicular transport is increased radially uniformly by a factor of 100 in the case of ion and electron thermal conductivity and 30 in the case of particle diffusivity from the inter-ELM ion neo-classical level. In the SOL on the 2D grid, the perpendicular transport enhancement is distributed poloidally according to a narrow Gaussian distribution (half width $\pi/16$ in terms of poloidal angle) centred at the outer midplane, as shown in Fig. 1a. At the separatrix, the poloidal average of the Gaussian distribution matches the level of thermal conductivity and particle diffusivity, respectively, in the ETB. In initial simulations, the Gaussian-shaped thermal conductivity and particle diffusivity distributions have simply been extended uniformly throughout the SOL, as illustrated by the blue curve in Fig. 1b, which shows different profiles for perpendicular transport used in the SOL. Figure 1c, which shows plots of the ion and electron heat fluxes to the wall as a function of time in the case of radially uniform perpendicular transport in the SOL, reveals the problem with this assumption: The heat fluxes to the wall are enormous, especially the ion heat flux, whereby very little power actually goes to the divertor plates [6]. Transport across the field lines, especially in the case of the ions, is faster than the parallel transport along the field lines by far. Since most of the power is actually deposited on the divertor plates in real experiments, the assumption of radially uniform perpendicular transport in the SOL seems to be inadequate. As a better approximation, a step-function shaped profile with a very low level of enhancement in the outer half of the SOL has been used in subsequent simulations. This more useful enhancement profile is illustrated by the red curve in Fig. 1b.

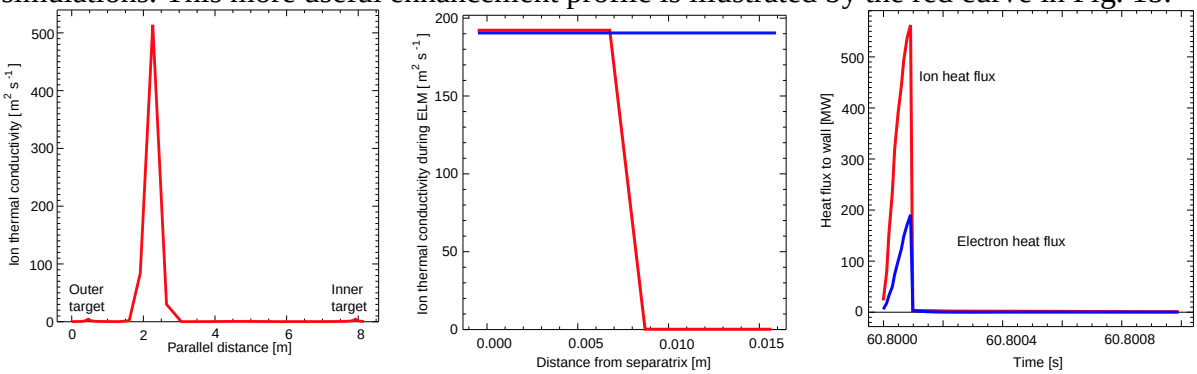

Figure 1. (a) Perpendicular ion thermal conductivity just outside the separatrix during an ELM as a function of the poloidal distance. (b) Perpendicular ion thermal conductivity in the SOL as a function of the radial coordinate during an ELM in two different scenarios, one with radially uniform perpendicular transport and one with radially step function-shaped perpendicular transport. (c) Ion and electron heat flux to the wall as a function of time in the case of radially uniform enhancement of perpendicular transport in the SOL.

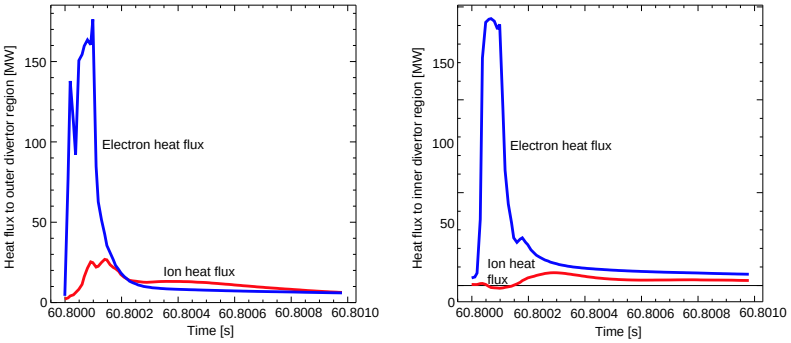

Figure 2. Ion and electron heat fluxes going to (a) the outer divertor region and (b) the inner divertor region in the simulation with radially step-function-shaped enhancement of perpendicular transport in the SOL.

3. Results. Figures 2a and 2b show the ion and electron heat fluxes at the outer and inner targets as a function of time in the simulation with the step-function-shaped enhancement of radial perpendicular transport in the SOL. Contrary to expectations, the ion heat fluxes measured at both targets are still rather small compared to the electron heat fluxes. The reason

for this discrepancy turns out to be strong ion-electron equipartition.

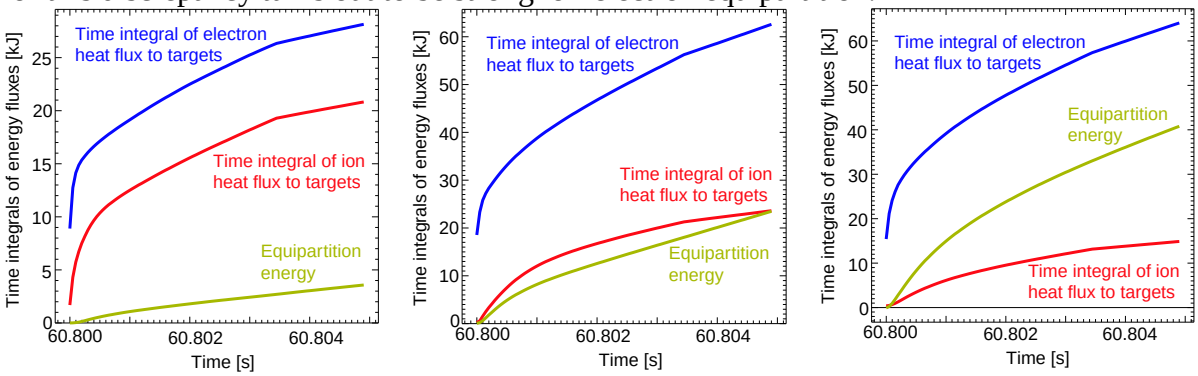

Figure 3. Time integrals of the total ion heat flux measured at both targets, the total electron heat flux measured at both targets and the volume-integrated ion-electron equipartition energy as a function of time for three simulations with the following separatrix densities: (a) 8×10^{18} m^{-3}, (b) 1.7×10^{19} m^{-3} and (c) 4.0×10^{19} m^{-3}.

Further simulations show that the ion-electron equipartition varies strongly as a function of the plasma parameters. The higher the density, the larger a fraction of the total energy carried by the ions is transferred to the electrons. This is illustrated in Fig. 3, which shows time integrals of the total ion heat flux measured at both targets, the total electron heat flux measured at both targets and the volume-integrated ion-electron equipartition energy as a function of time for three simulations with different densities. Figure 3a corresponds to a simulation with an average separatrix density of 8×10^{18} m^{-3}, Fig. 3b to a simulation with an average separatrix density of 1.7×10^{19} m^{-3} and Fig. 3c to a simulation with an average separatrix density of 4.0×10^{19} m^{-3}. The sequence of figures clearly shows how the amount of energy carried by the ions relative to that carried by the electrons decreases, as the ion-electron equipartition energy increases with the density.

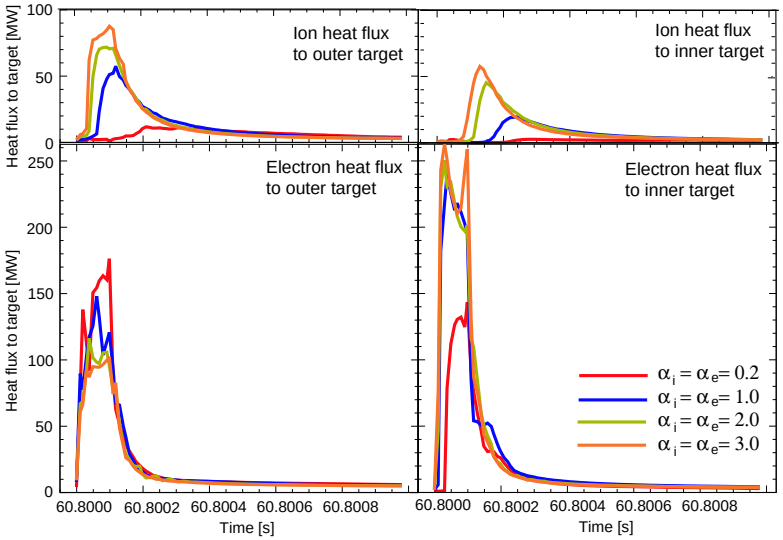

Figure 4. Ion and electron heat fluxes at the outer and inner targets for four different values of the parallel heat flux limiting factors.

The sensitivity of the heat fluxes measured at the targets to the assumptions about perpendicular transport and to the plasma parameters suggests that parallel transport might also be important. Therefore, the effect of varying the parallel heat flux limiting factors have been studied. In Fig. 4, for different levels of the flux limiting factors have been used: $\alpha_i = \alpha_e = 0.2$, $\alpha_i = \alpha_e = 1.0$, $\alpha_i = \alpha_e = 2.0$, $\alpha_i = \alpha_e = 3.0$. The figure shows how the ion and electron heat fluxes at the outer and inner targets vary for the different values of the flux limiting factors. It should be noticed that especially the ion heat fluxes vary significantly as a function of the heat transmission factors and that about $\alpha_i = \alpha_e = 1.0$ is needed for a significant response to be seen at the outer target and about $\alpha_i = \alpha_e = 2.0$ for a sizeable response at the inner target. This suggests that using *ad hoc* constant flux limiting factors is not a very sensible approach. Furthermore, it demonstrates that the fluid approach alone is insufficient for accurately model-

ling transients, since it cannot determine the flux limiting factors self-consistently. Instead, the flux limiting expressions have to be calculated kinetically during transients.

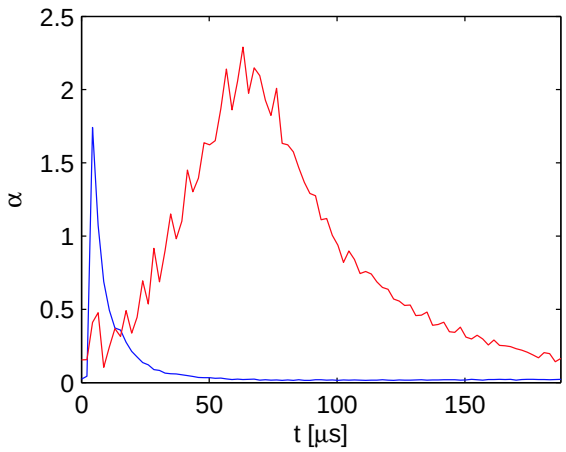

Figure 5. The parallel flux limiting factors α_i (red curve) and α_e (blue curve) as a function of time during an ELM in a low-recycling JET plasma.

At present, the parallel heat flux limiting factors are being calculated in particle-in-cell (PIC) simulations with the BIT1 PIC code [7] for a number of relevant transient scenarios. The kinetically calculated heat transmission factors are being used in the integrated transport simulations. Initially, only a time dependency is assumed for the heat transmission factors, but later the spatial dependency of them will also be taken into account. Figure 5 shows some initial results of how the heat flux limiting factors vary over time during an ELM in a low recycling JET ELMy H-mode plasma. It is clearly seen that the transmission factors vary greatly with time during the transient.

4. Conclusions. Overall, this study shows that the heat fluxes at the targets and at the wall depend very sensitively on the assumptions of both perpendicular and parallel transport in the SOL during and after an ELM. In particular, too large radial transport in the outer part of the SOL during the ELM leads to an enormous heat flux to the wall. It has been shown that the ions generally lose energy to the electrons at a fast rate during the transient. The ion-electron equipartition increases strongly with the density. Through PIC simulations, it has also been demonstrated that the parallel heat flux limiting factors vary strongly during transients, whereby the fluid approach alone is insufficient for obtaining self-consistent modelling results. An integrated fluid-kinetic approach is being devised, which involves calculating the flux limiting factors kinetically in PIC simulations of the transient scenarios.

[1] A. Loarte *et al*., Plasma Phys. Control. Fusion **44** 1815 (2002).
[2] G. Cennachi, A. Taroni, JET Report JET-IR(88)03 (1988).
[3] R. Simonini *et al*., Contrib. Plasma Phys. **34** 368 (1994).
[4] J.-S. Lönnroth *et al*., Plasma Phys. Control. Fusion **45** 1689 (2003).
[5] G.J. Radford "Classical parallel transport in a multi-species plasma from a 21 moment approximation", JET Report JET-R(93)05 (1993).
[6] J.-S. Lönnroth *et al*., Proc. 31st EPS Conference on Plasma Physics and Controlled Fusion (2004).
[7] D. Tskhakaya, S. Kuhn, Contrib. Plasma Phys. **42** 302 (2002).